Electronic Supplementary Material (ESI) for ChemComm.

Supporting Information

Ferrocene-modified stable metal-organic framework for efficient CO_2 photoreduction reaction

Gui-Qi Lai[†a], Ning Li[†a], Jun He[*a], and Ya-Qian Lan[*b]

[a]School of Chemical Engineering and Light Industry, Guangdong University of Technology, Guangzhou 510006, Guangdong, China.

[b]School of Chemistry, South China Normal University, Guangzhou 510006, PR China.

[†]These authors contributed equally.

Email: junhe@gdut.edu.cn; yqlan@m.scnu.edu.cn

Experimental Procedures

Materials

All chemicals and reagents were purchased commercially without further purification. Ferrocenecarboxaldehyde (Fca), Ferrocence (Fc), 2-Amino-1,4-benzene dicarboxylic acid (H_2aBDC, 99.0%), Nafion (5% w/w in water and 1-propanol) were purchased from Alfa Aesar. Titanium tetraisopropanolate (Ti(O*i*Pr)$_4$, 95%), Triethanolamine (TEOA, 99%) were purchased from Aladdin. N,N-dimethylformamide (DMF, 99.5%), methanol (CH_3OH) and triethylamine (Et_3N, 99.0%) were purchased from Admas.

Instruments

Fourier-transform infrared (IR spectra (4000-500 cm^{-1}) were obtained in KBr discs on a Thermo Nicolet IS50 FTIR spectrometer. UV-Vis-NIR diffuse reflectance spectra (UV-Vis-NIR DRS) was recorded on a Varian Cary 5000 in the wavelength range of 250-800 nm. Powder X-ray diffraction (PXRD) spectra were carried out on a Rigaku Smart Lab diffractometer. Thermogravimetric analyses were performed on a Diamond DSC Pyris 1 analyzer. CO_2 adsorption and desorption isotherms were determined by Autosorb IQ2 (Quantachrome Instruments). X-ray photoelectron spectroscopy (XPS) was recorded using Escalab 250Xi instrument.

Synthesis methods

Synthesis of NM.

NM was synthesized by previous literature. 3 mmol (543 mg) of H_2aBDC and 0.75 mmol (0.26 mL) of Ti(O*i*Pr)$_4$ were dissolved in 1.0 mL of methanol and 9.0 mL of DMF. The solution was stirred for 30 min, and then transferred into a 50 mL Teflon-lined stainless for 72h at 150℃. After the reaction was cooled to room temperature, light yellow microcrystalline power was collected by centrifugation and washed with DMF and methanol. The solid was dried in a vacuum oven at 80°C for 12 h.

Synthesis of FNM-1

0.3 mmol (64.2 mg) of Fca (N_{NH2}：N_{Fca}=1:1) was dissolved in 10.0 mL of methanol, 0.05 mmol (84.7 mg) of **NM** was added into 10.0 mL of methanol and stirred. Then the dissolved Fca solution was slowly added to **NM** solution, the mixed solution stirred for 30 min. Finally, 42 μL of Et_3N was slowly added to the above mixed solution and stirred overnight at room temperature. The resulting dark gray turbid solution was collected by centrifugation and washed with methanol solvent several times until the color of the solution was colorless, then the microcrystalline samples were dried in a vacuum oven at 80 °C for 12 h.

Synthesis of FNM-2

FNM-2 samples were achieved by almost the same process as that of **FNM-1**, except using 3.0 mmol (642.2mg) of Fca (N_{NH2}：N_{Fca}=1:10) and 210 μL of Et_3N.

Synthesis of F@NM

The synthetic process is similar as that of **FNM-1**, except that **NM** crystals was added into 10.0 mL of methanol with 1.5 mmol (279.0 mg) Fc and stirred for 12 h. The resulting solution was collected by centrifugation and washed with methanol solvent several times until the color of the solution was colorless, then the microcrystalline samples were dried in a vacuum oven at 80 °C for 12 h.

The generalization of the synthetic scheme

To demonstrate that this strategy is also applicable to other amino-functionalized MOFs, we prepared ferrocene-grafted NH_2-UiO-66 using a similar synthetic approach, i.e., an aldehyde-amine condensation reaction using ferrocenecarboxaldehyde (Fca) and NH_2-UiO-66 microcrystals.

The relevant synthesis method is as follows:

Synthesis of NH_2-UIO-66

NH_2-UIO-66 was synthesized by previous reference with slightly modified method[a]. Typically, NH_2BDC (0.5275 mmol) and $ZrCl_4$ (0.5675 mmol) were dispersed in 25 mL DMF and 875 μL CH_3COOH by ultrasonic treatment for 30 min. This solution was transferred into a 50 mL Teflon-lined stainless steel autoclave for 1 days at 120 °C under autogenous pressure. After cooling down to room temperature, pale pink powders were collected by filtration and fully washed several times with DMF.

[a] Li, Z.; Zhao, S.; Wang, H.; Peng, Y.; Tan, Z.; Tang, B. Functional groups influence and mechanism research of UiO-66-type metal-organic frameworks for ketoprofen delivery. *Colloids Surf. B. Biointerfaces* **2019,** *178*, 1.

Synthesis of FN-UIO-66

0.3 mmol (64.2 mg) of Fca was dissolved in 10.0 mL of methanol, 0.03 mmol (52.5mg) of NH_2-UIO-66 was added into 10.0 mL of methanol and stirred. Then the dissolved Fca solution was slowly added to NH_2-UIO-66 solution, the mixed solution stirred for 30 min. Finally, 42 μL of Et_3N was slowly added to the above mixed solution and stirred overnight at room temperature. The resulting reddish brown turbid solution was collected by centrifugation and washed with methanol solvent several times until the color of the solution was colorless, then the microcrystalline samples were dried in a vacuum oven at 80℃ for 12 h.

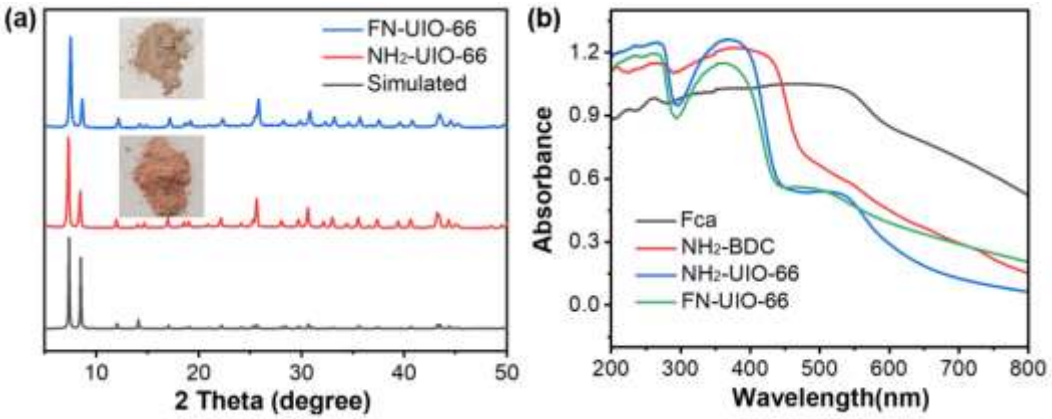

(a) Power XRD patterns of NH_2-UiO-66 and FN-UiO-66; (b) UV/Vis-NIR DRS spectra of Fca ligand, NH_2-BDC, NH_2-UIO-66 and FN-UIO-66.

As shown in Figure R1, compared to the pristine NH_2-UiO-66 structure, the ferrocene-grafted MOF not only maintains the parent framework, but also shows an improvement in light-harvesting ability (*ca*. 550-800 nm), which is consistent with the phenomenon in our work. These results suggest that this strategy can indeed be applied to other amino-functionalized MOFs.

Photocatalytic CO_2 reduction experiments

The activated **NM**、**FNM-1-2** and **F@NM** were used as photocatalysts to carry out CO_2 reduction reaction. Photocatalyst (5mg) was added into H_2O (28 mL) with Triethanolamine (TEOA, 2 mL) as the sacrificial agent. After degassing with high-purity CO_2 for 30 minutes, the reaction was carried out under a 300 W Xe lamp with UV and a cut filter to keep the wavelengths ranging from 420 to 800 nm. The reaction temperature was controlled at 25℃ by using the cooling water circulation. The photocatalytic gas products (CO, CH_4, O_2, H_2.etc.) were detected by gas chromatograph (GC) with a flame ionization detector (FID) and a thermal conductivity (TCD) detector to analyze the different gases. The liquid products (HCOOH) were measured using ion chromatography (IC).

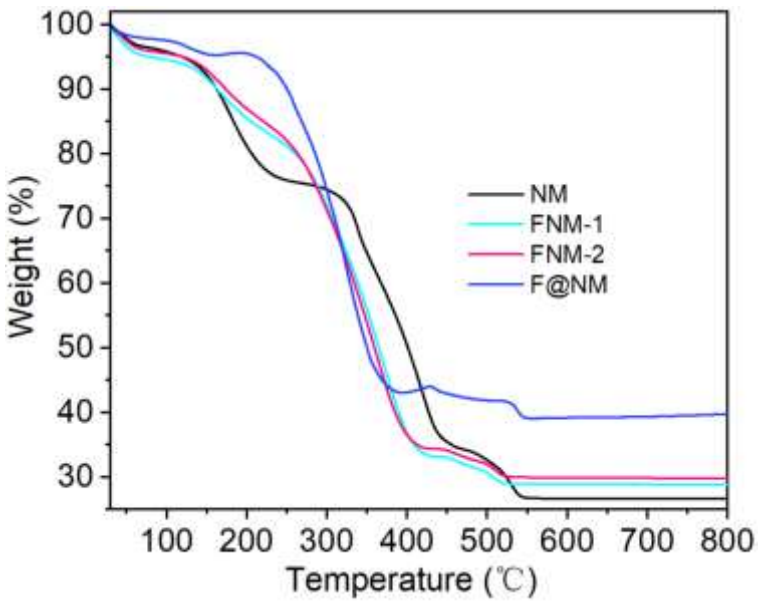

Figure S1. The thermogravimetric analysis of **NM** (black), **FNM-1** (cyan), **FNM-2** (pink), **F@NM** (blue). Compared to **NM**, several other ferrocene-grafted or loaded MOF-based materials have significantly higher residual oxide solid masses, and the order of the residual solid masses is **F@NM** > **FNM-2** > **FNM-1** > **NM**, which is consistent with the synthetic feed ratio of the reactants.

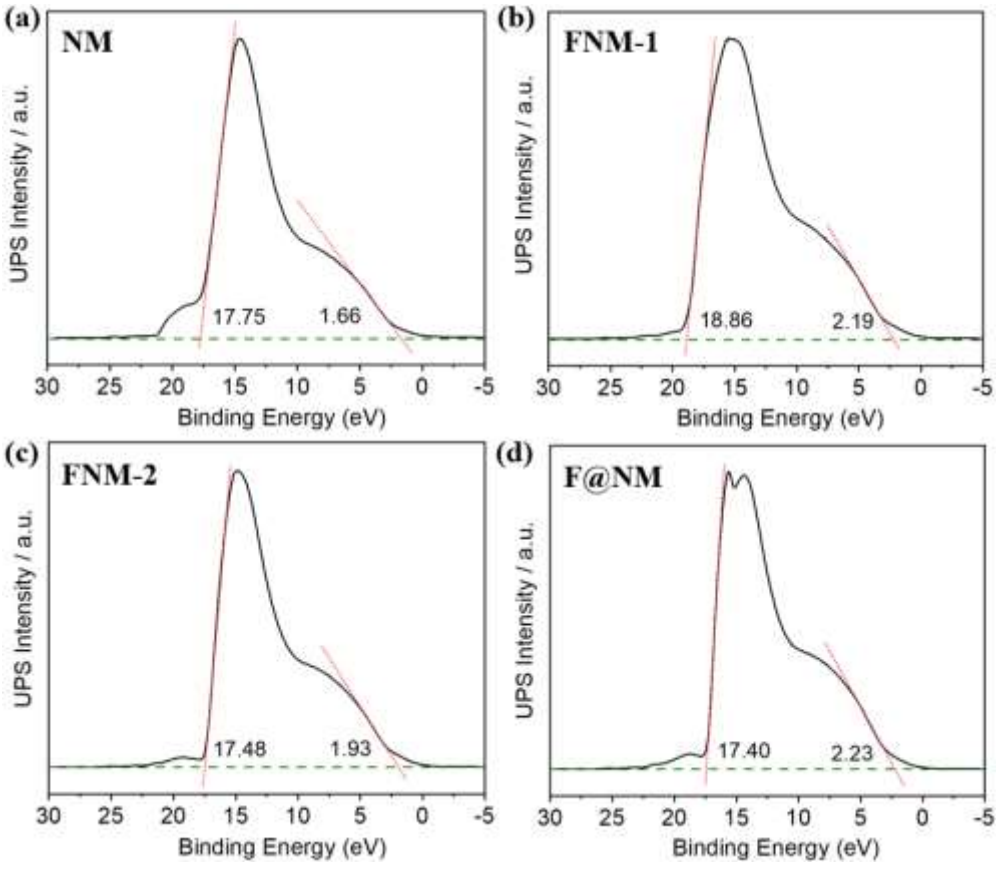

Figure S2. UPS spectra of **NM**、**FNM-1**, **FNM-2** and **F@NM**

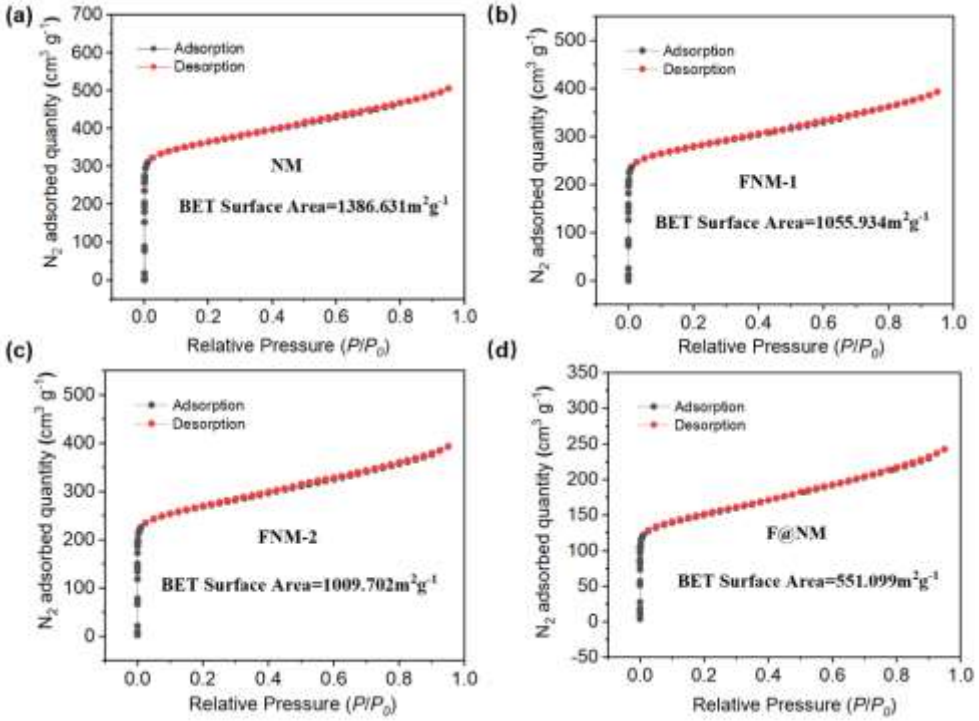

Figure S3. N_2 adsorption-desorption isotherms of **NM**、**FNM-1**, **FNM-2** and **F@NM** compounds. The BET surface areas of **FNM-1-2** and **F@NM** were found to be 1055.93,1009.70 and 551.10 $m^2 g^{-1}$.

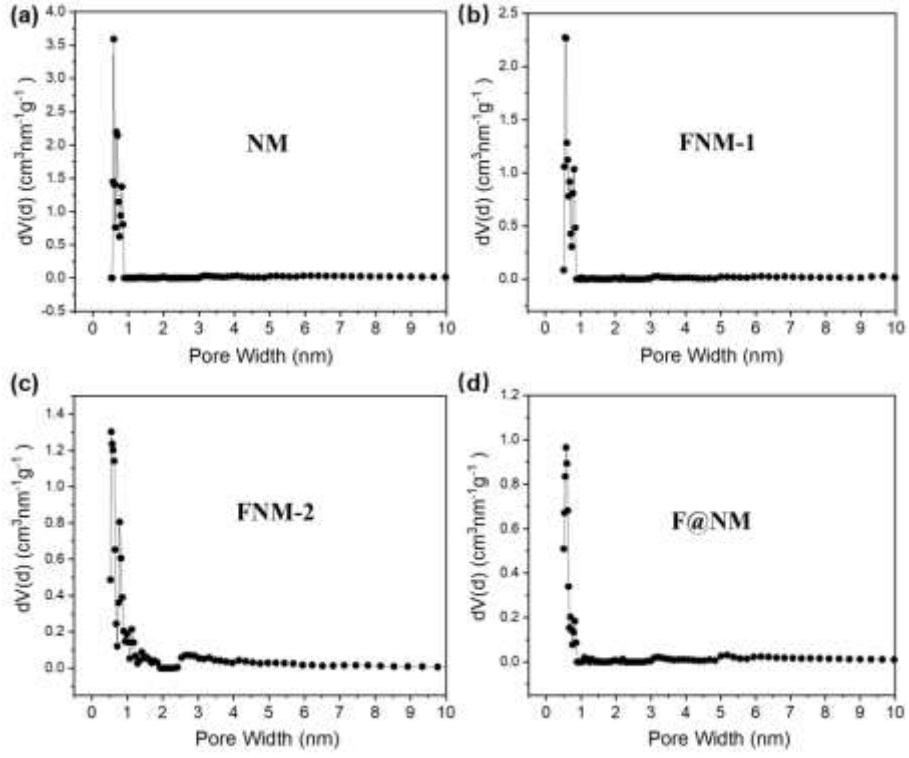

Figure S4. The pore size distributions for **NM**, **FNM-1**, **FNM-2** and **F@NM**. The pore volume of

MOF decreases gradually with increasing grafting/loading amount of ferrocenes.

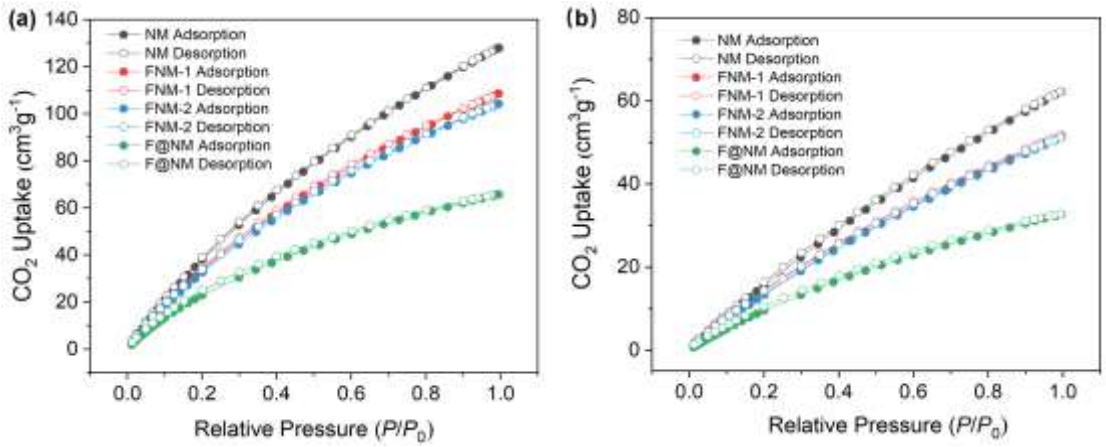

Figure S5. The CO_2 sorption isotherms of **NM**, **FNM-1**, **FNM-2** and **F@NM** at (a) 273K and (b) 298 K. grafting or loading of ferrocenes blocked the porosity of MOF, which led to the decrease in CO_2 adsorption compared to the parent MOF (i.e. NM). Meanwhile, the loading of ferrocenes in the MOF structure is higher than the grafting amount, so the decrease of CO_2 adsorption is more obvious.

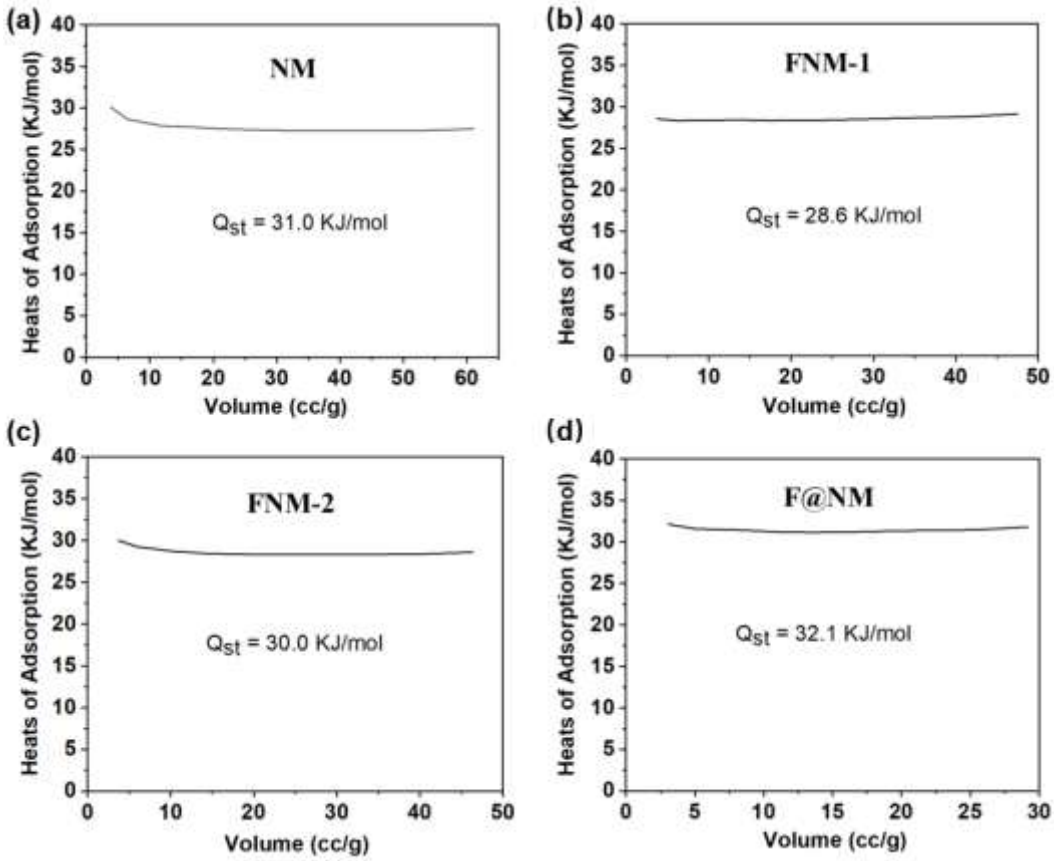

Figure S6. The heat adsorption (Qst) of **NM**, **FNM-1**, **FNM-2** and **F@NM**.

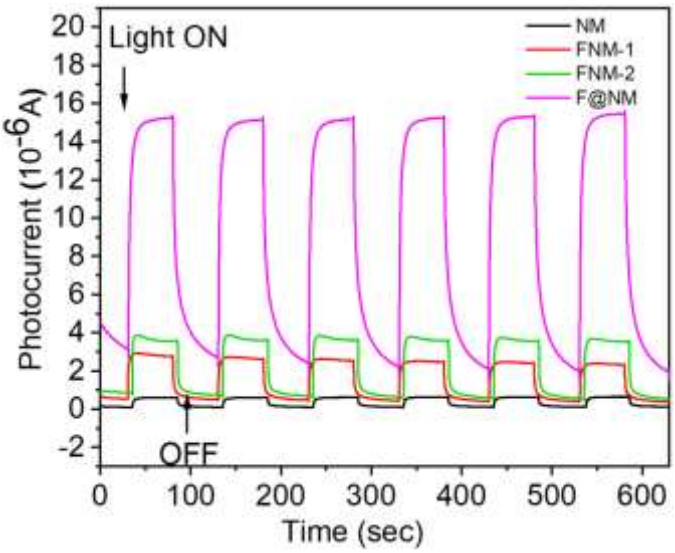

Figure S7. Transient photocurrent response of **NM**、**FNM-1**, **FNM-2** and **F@NM**. A Xenon light (400-800 nm) as the light source was applied for photocurrent measurement, and 0.5 M Na_2SO_4 aqueous solution was used as the electrolyte.

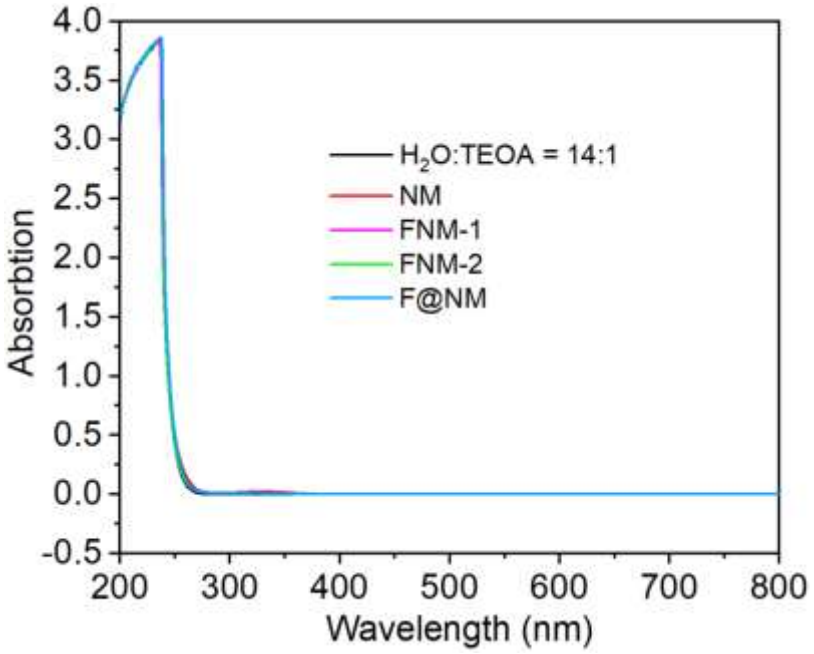

Figure S8. Absorption spectra of filtrate for **NM**、**FNM-1**, **FNM-2** and **F@NM** reactive solution after photocatalytic reaction. There is no other obvious absorption peak noticed.

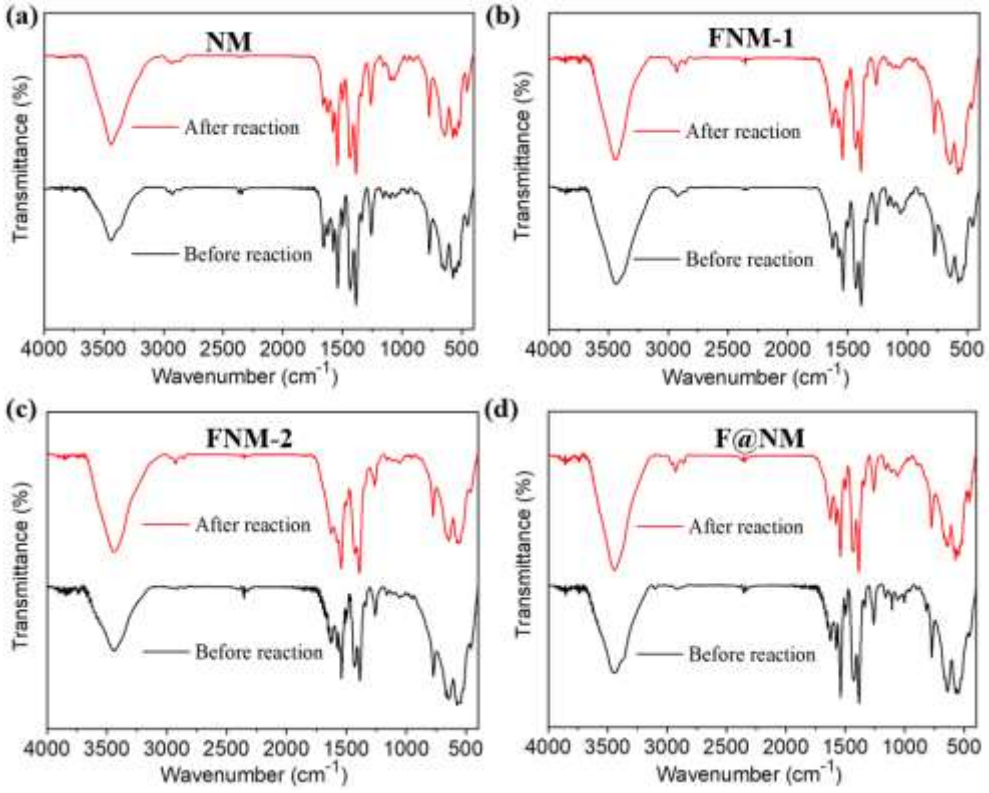

Figure S9. FTIR spectroscopy of **NM**、**FNM-1**, **FNM-2** and **F@NM** compounds before (black curve) and after (red curve) photocatalytic reaction test.

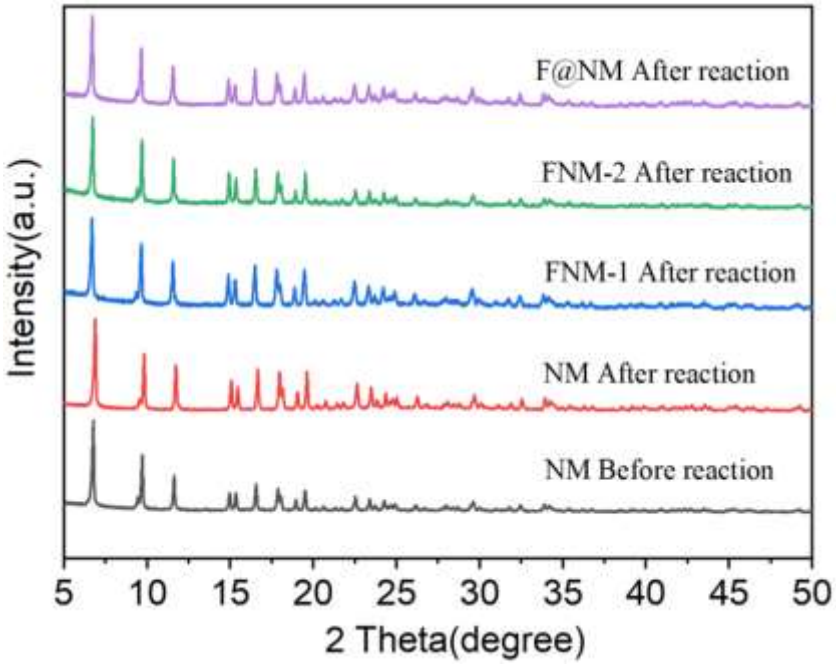

Figure S10. PXRD patterns of **NM**、**FNM-1**, **FNM-2** and **F@NM** after photocatalytic reaction test. There is no other absorption peak appeared, determining that these crystal structures are stable.

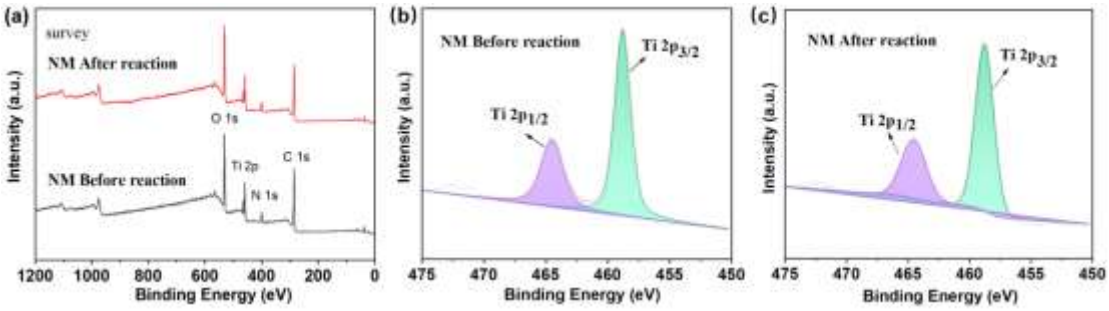

Figure S11. The full-scan and high-resolution XPS spectra of **NM** before and after reaction.

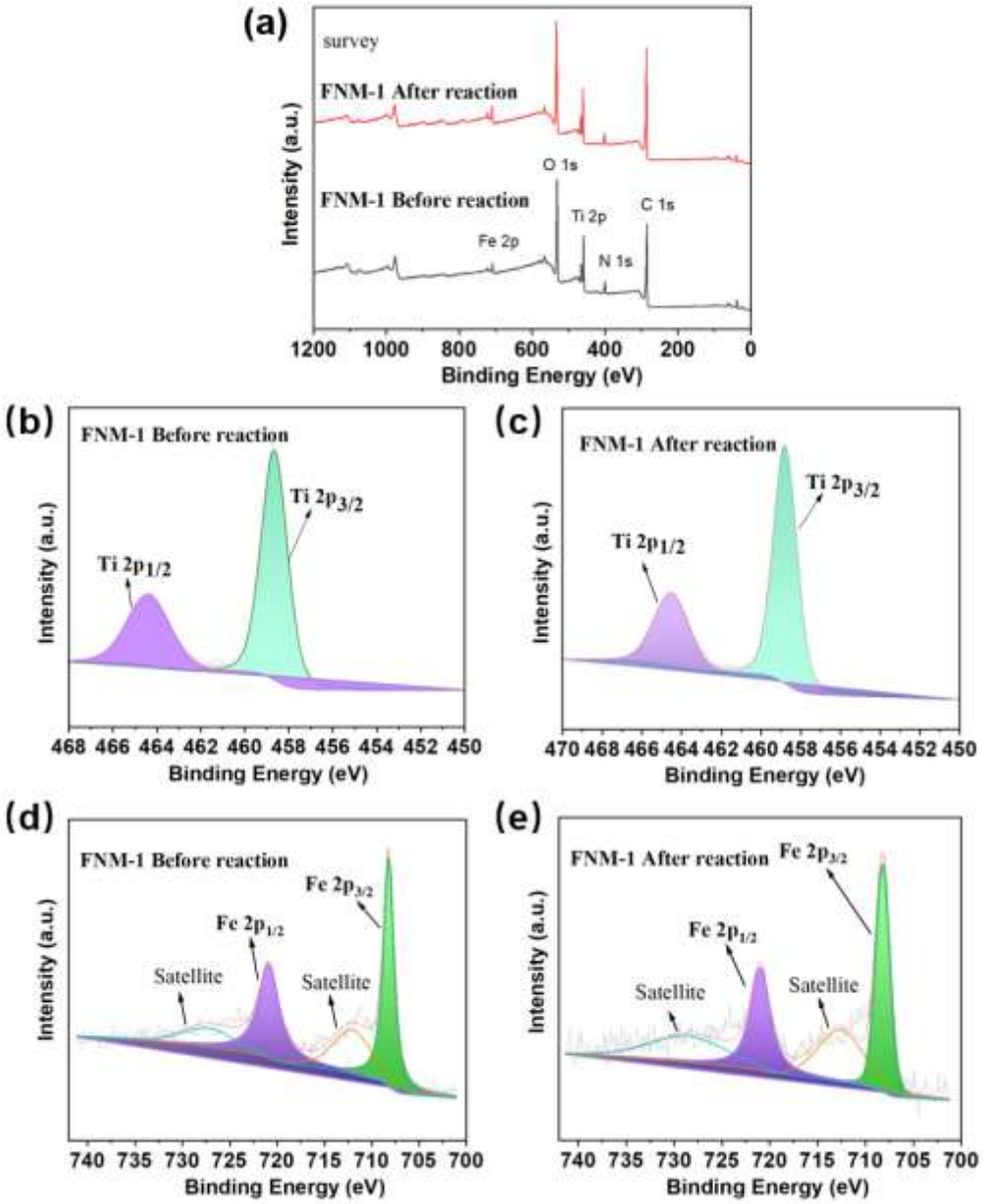

Figure S12. The full-scan and high-resolution XPS spectra of **FNM-1** before and after reaction.

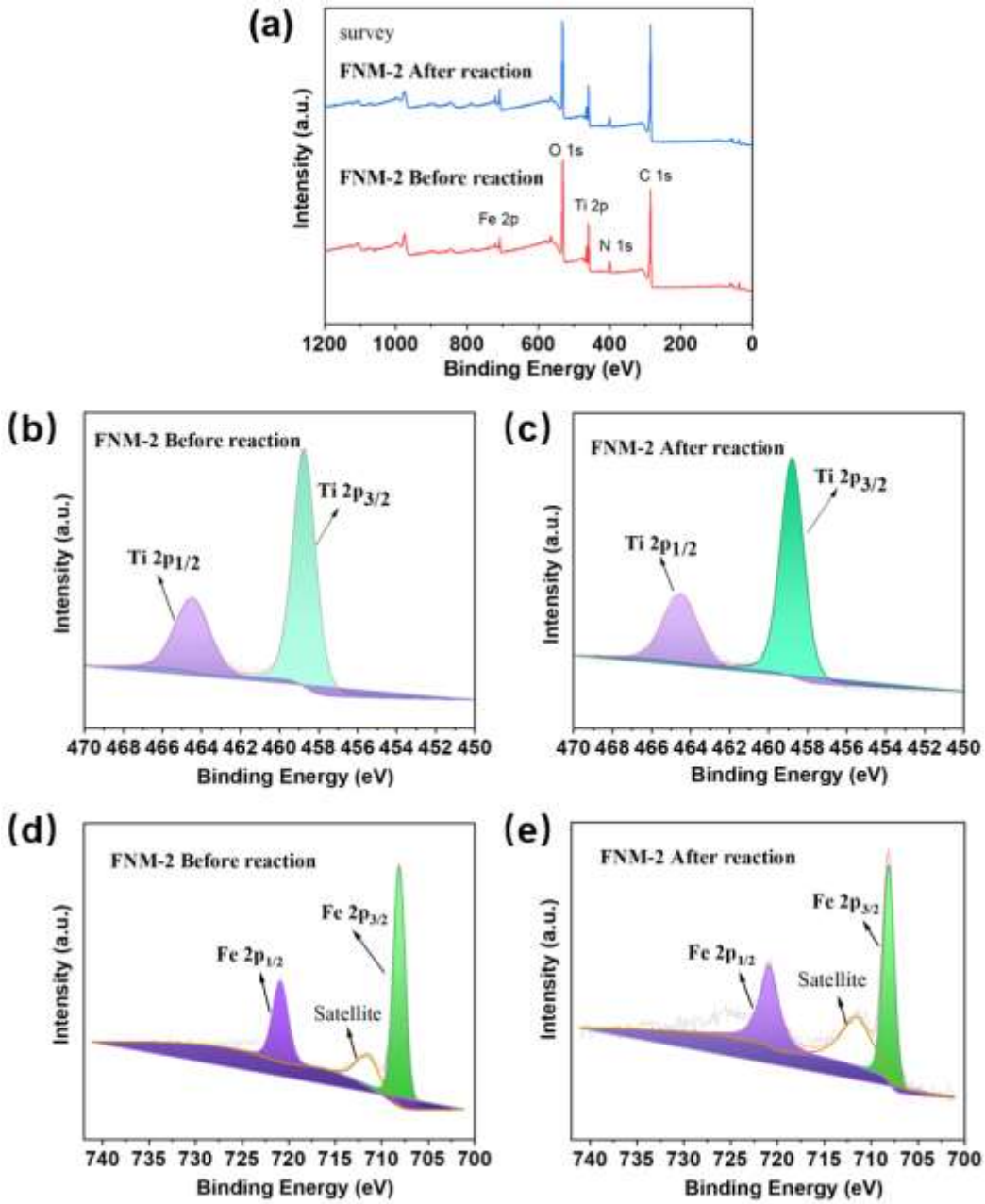

Figure S13. The full-scan and high-resolution XPS spectra of **FNM-2** before and after reaction.

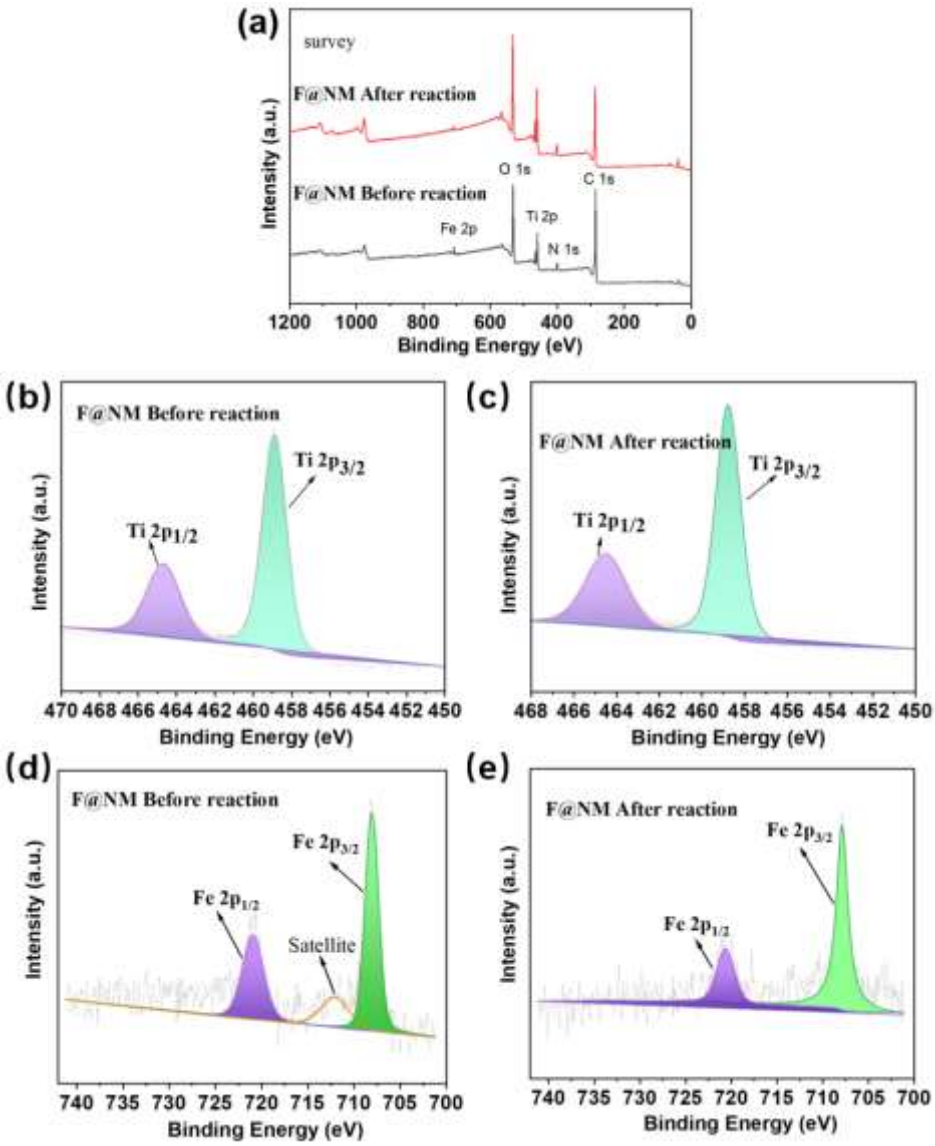

Figure S14. The full-scan and high-resolution XPS spectra of **F@NM** before and after reaction.

The X-ray photoelectron spectroscopy (XPS) characterization was further performed to identify the chemical valence states of Ti and Fe atoms of these MOFs before and after photocatalytic reaction. As shown in Figure S11, the Ti 2p spectrum of NM exhibits that the peak at 458.8 eV is the state of Ti $2p_{2/3}$, while the peak at 464.6 eV refers to the state of Ti $2p_{1/2}$. Moreover, the binding energies of Ti $2p_{2/3}$ and Ti $2p_{1/2}$ before and after photocatalytic reaction are almost unchanged, indicating the high structural stability of NM. For ferrocene-based MOF photocatalysts (**FNM-1**, **FNM-2** and **F@NM**), their Ti 2p and Fe 2p spectra also keep the same before and after reaction, as demonstrated in Figure S12-S14. The high-resolution Fe 2p spectra of **FNM-1**, **FNM-2** and **F@NM** clearly display two characteristic peaks of 708.1 eV (Fe $2p_{2/3}$) and 720.9 eV (Fe $2p_{1/2}$), which indicates the unique existence of Fe^{2+} in these MOFs.

Table S1. Control experiments under different conditions for the photocatalytic CO_2 reduction reaction.

Entry 1	**[b]HCOOH (μmol)**	**[c]CO (μmol)**	**[d]H_2 (μmol)**
NM	7.58	0.11	0
1[e]	n.d. [f]	n.d. [f]	n.d. [f]
2[g]	n.d.	n.d.	n.d.
3[h]	n.d.	n.d.	n.d.
4[i]	n.d.	n.d.	Trace amount
Entry 2	**[b]HCOOH (μmol)**	**[c]CO (μmol)**	**[d]H_2 (μmol)**
FNM-1	10.66	0.27	0
1[e]	n.d. [f]	n.d. [f]	n.d. [f]
2[g]	n.d.	n.d.	n.d.
3[h]	n.d.	n.d.	n.d.
4[i]	n.d.	n.d.	Trace amount
Entry 3	**[b]HCOOH (μmol)**	**[c]CO (μmol)**	**[d]H_2 (μmol)**
FNM-2	14.76	0.66	0
1[e]	n.d. [f]	n.d. [f]	n.d. [f]
2[g]	n.d.	n.d.	n.d.
3[h]	n.d.	n.d.	n.d.
4[i]	n.d.	n.d.	Trace amount
Entry 4	**[b]HCOOH (μmol)**	**[c]CO (μmol)**	**[d]H_2 (μmol)**
F@NM	8.45	0.71	0
1[e]	n.d. [f]	n.d. [f]	n.d. [f]
2[g]	n.d.	n.d.	n.d.
3[h]	n.d.	n.d.	n.d.
4[i]	n.d.	n.d.	Trace amount

[a] Reaction conditions: catalyst (entry 1 is activated **NM**, entry 2 is activated **FNM-1**, entry 3 is

activated **FNM-2**, entry 4 is activated **F@NM**; H_2O (28 mL), TEOA (2 mL); CO_2 (1 atm); λ = 200-400 nm (UV light); 30 °C, 10 h. [b] The HCOOH production rate. [c] The CO production rate. [d] The H_2 production rate. [e] In the dark. [f] Not detectable (n.d.). [g] Without catalyst. [h] Without TEOA. [i] Using N_2 to replace CO_2.

Table S2. Comparison of the photocatalytic performance of reported photocatalysts for CO_2-to-HCOOH conversion under visible light irradiation.

Photocatalyst	Solvent	PS/PM	SA	HCOOH(μmol/g/h)	Reference
NM	H_2O	None	TEOA	67.33[a]; 151.60 [b]	this work
FNM-1	H_2O	None	TEOA	136.33 [a]; 213.20 [b]	this work
FNM-2	H_2O	None	TEOA	266.33[a]; 293.40 [b]	this work
F@NM	H_2O	None	TEOA	88.66[a]; 169.00 [b]	this work
NH_2-MIL-125(Ti)	MeCN	None	TEOA	16.28	[1]
NH_2-MIL-101(Fe)	MeCN	None	TEOA	445	[2]
NH_2-MIL-53(Fe)	MeCN	None	TEOA	116.25	[2]
NH_2-MIL-88B(Fe)	MeCN	None	TEOA	75.0	[2]
H_2N-UIO-66(Zr)	MeCN	None	TEOA	46.3	[3]
UiO-66-(Zr/Ti)-NH_2	MeCN	None	TEOA	5.8 mmol mol^{-1}	[4]
NNU-28	MeCN	None	TEOA	183.3	[5]
PCN-222	H_2O	None	TEOA	143.5	[6]
AD-MOF-1	MeCN	None	TIPA	179.0	[7]
AD-MOF-2	H_2O	None	TIPA	443.2	[7]
COF-367-Co^{II}	MeCN	None	TEA	48.6	[8]
COF-367-Co^{III}	MeCN	None	TEA	93.0	[8]
CTF	PBS	Rh[Cp*Rh(bpy)H_2O]	Vc	881.3 × 10^3	[9]
TpBD–H_2	MeCN	None	TEOA	45.7	[10]
TpBD–$(CH_3)_2$	MeCN	None	TEOA	86.3	[10]
TpBD–$(OCH_3)_2$	MeCN	None	TEOA	108.3	[10]
TpBD–$(NO_2)_2$	MeCN	None	TEOA	22.2	[10]

MCOF-Ti_6Cu_3	H_2O	None	None	169.8	[11]
DQTP COF-Co	MeCN	$Ru(bpy)_3Cl_2·6H_2O$	TEA	34.87μmol	[12]
DQTP COF-Co	MeCN	$Ru(bpy)_3Cl_2·6H_2O$	TIPA	33.38μmol	[12]
DQTP COF-Co	H_2O	$Ru(bpy)_3Cl_2·6H_2O$	TEOA	94.68μmol	[12]

PS: photosensitizer; PM: precious metal; SA: sacrificial agent TEOA: triethanolamine; TIPA: triisopropanolamine; PBS: sodium phosphate buffer; Vc: ascorbic acid; TEA: triethylamine.
[a]Reaction conditions: Visible light
[b]Reaction conditions: λ = 200-400 nm (UV light)

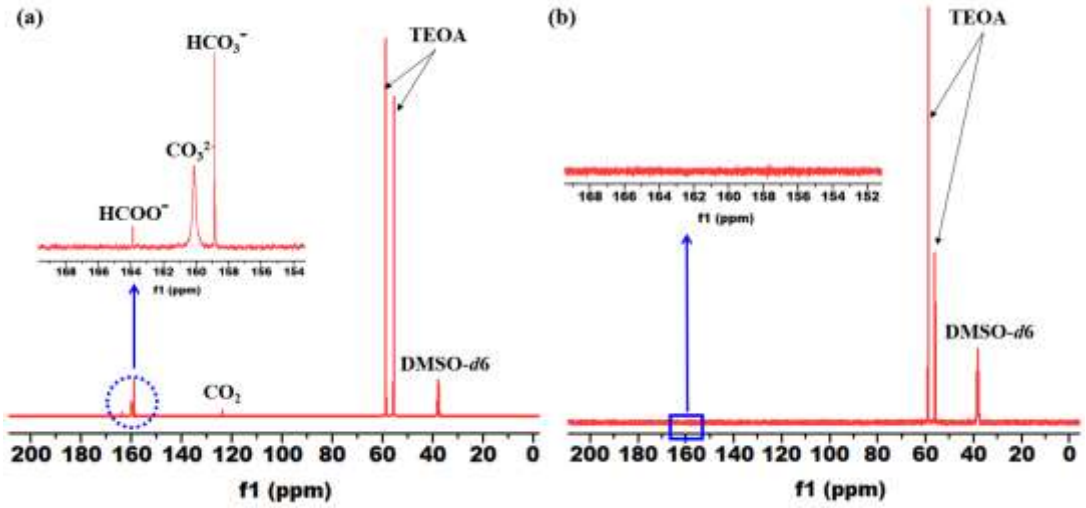

Figure S15. (a) ^{13}C NMR spectrum of reaction solution catalyzed with **FNM-2** photocatalyst under $^{13}CO_2$ atmosphere, the $HCOO^-$ signal at 163.9 ppm was clearly observed. (b) ^{13}C NMR spectroscopy for the liquid products obtained from reaction with $^{12}CO_2$. Peaks that do not show any product.

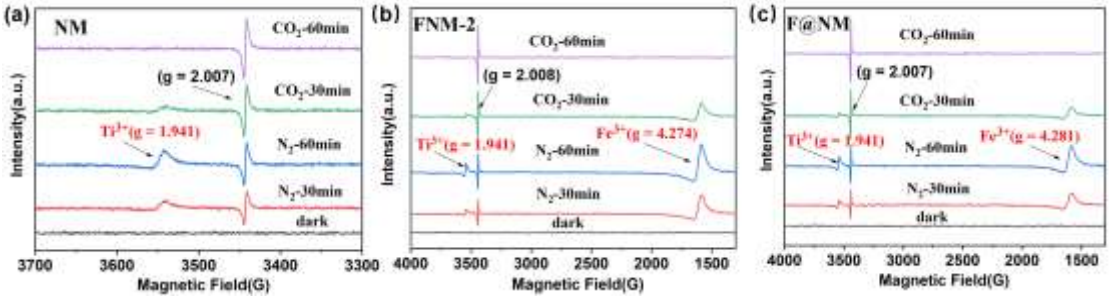

Figure S16. EPR spectra of **NM**, **FNM-2** and **F@NM** under UV light irradiation and a CO_2 or N_2 atmosphere.

Reference

(1) Y. Fu, D. Sun, Y. Chen, R. Huang, Z. Ding, X. Fu, and Z. Li. *Angew. Chem. Int. Ed.* **2012**, *51*, 3364 –3367.

(2) D. Wang, R. Huang, W. Liu, D. Sun, and Z. Li. *ACS Catal*. **2014**, *4*, 4254 −4260.

(3) D. Sun, Y. Fu, W. Liu, L. Ye, D. Wang, L. Yang, X. Fu, and Z. Li. *Chem. Eur. J*. **2013**, *19*, 14279 –14285.

(4) D. Sun, W. Liu, M. Qiu, Y. Zhang, Z. Li. *Chem. Commun.*, **2015**, *51*, 2056 –2059.

(5) D. Chen, H. Xing, C. Wang and Z. Su. *J. Mater. Chem. A*, **2016**, *4*, 2657 – 2662.

(6) H.-Q. Xu, J. Hu, D. Wang, Z. Li, Q. Zhang, Y. Luo, S.-H. Yu, and H.-L. Jiang. *J. Am. Chem. Soc*. **2015**, *137*, 13440 −13443.

(7) N. Li, J. Liu, J. J. Liu, L. Z. Dong, Z. F. Xin, Y. L. Teng and Y. Q. Lan. *Angew. Chem. Int. Ed.*, **2019**, 58, 5226 –5231.

(8) Y.-N. Gong, W.-H. Zhong, Y. Li, Y.-Z. Qiu, L.-R. Zheng, J. Jiang, and H.-L. Jiang. *J. Am. Chem. Soc.* **2020**, *142*, 16723–16731.

(9) R. K. Yadav , A. Kumar , N.-J. Park , K.-J. Kong and J.-O. Baeg. *J. Mater. Chem. A*, **2016**, ***4*** , 9413 –9418.

(10) L. Peng, S. Chang , Z. Liu , Y. Fu , R. Ma , X. Lu , F. Zhang , W. Zhu , L. Kong and M. Fan. *Catal. Sci. Technol.*, **2021**, ***11***, 1717–1724.

(11) J. Zhou, J. Li, L.K, L. Zhang, Q. Huang, Y. Yan, Y.-F. Chen, J. Liu, S.-L. Li, and Y.-Q. Lan. *Nat. Commun.*, **2022** *13:*4681.

(12) M. Lu, Q. Li, J. Liu, F.-M. Zhang, L. Zhang, J.-L. Wang, Z.-H. Kang, and Y.-Q. Lan. *Appl. Catal. B Environ.*, **2019**, *254*, 624–633.